Chapter 5. Source Waveform Estimation

The ray theory approximation and the wave equation approach to multiples suppression described in Chapters 2 and 3 both require an a priori knowledge of the source waveform. As mentioned in Chapter 2, once we know the source signature, we can go two ways: 1) either we can incorporate it into the computer algorithms as a boundary condition or 2) we can deconvolve the input data with the known waveform and assume in the algorithm a spike-like shot wavelet. In the first case, unless the waveform is guaranteed to be minimum phase, the algorithms become highly unstable. For this reason we prefer the second alternative.

Source waveform estimation has been a major problem in geophysics for quite a while and although several methods have been discussed in the literature no completely satisfactory answer to the problem exists. We do not have a completely satisfactory solution either and what follows should be considered as just the preliminary steps toward the proper incorporation of this very important parameter into our scheme for multiples suppression.

In this chapter I intend to discuss two procedures which, despite their limited range of applicability, fit well into our general approach to the problem of multiple suppression. The first one is based on the Noah algorithm of Chapter 2 and the second on a recursive optimization intended to minimize the power of the recorded seismogram. Both techniques are illustrated with synthetic and real examples.

5.1. Slanted Noah Waveform Estimation

Riley [17] briefly mentioned the possibility of computing the shot waveform in the case of deep water multiples from the same Noah algorithm. Below I describe an extension of Riley's ideas which is more consistent with our initial assumptions and input data. It incorporates slanted propagation and accounts for lateral variations of the waveforms and reflection coefficients. The technique is best described if we Z-transform our variables. We begin by assuming that we have a seismogram at the surface

$$R = \Sigma r_t z^t \tag{5-1}$$

where we can clearly differentiate the primaries within a gate that goes from N_1 to N_2

$$P = \sum_{N_1}^{N_2} r_t z^t \tag{5-2}$$

and the corresponding first order multiples in the gate N_3 to N_4

$$M = \sum_{N_3}^{N_4} r_t z^t \tag{5-3}$$

By "clearly differentiate" we mean that we can choose both gates so that they do not overlap $(N_3 > N_2)$ and that no new primaries come into the multiples gate. This situation is most likely to apply with deep sea bottom multiples. In other words, if

$$c = \Sigma\, c_t\, z^t \tag{5-4}$$

represents the reflection coefficient sequence, then we ask for $c_t \approx 0$ in the gate $N_3 \leq t \leq N_4$. Then if we designate

$$B = \Sigma\, b_t\, z^t \tag{5-5}$$

as the source waveform and

$$B^{-1} = H = \Sigma\, h_t\, z^t \tag{5-6}$$

as its inverse, according to Figure 5.1 we can approximately write

$$P_1 = B_0\, c_1 \tag{5-7a}$$

$$P_2 = B_1\, c_2 \tag{5-7b}$$

$$M_2 = -\, B_0\, c_1\, c_2 \tag{5-7c}$$

where 0, 1, 2 refer to different surface and sub-surface locations. Taken separately, relations (5-7) are only true for vertical propagation. Nevertheless, if the gates for P and M are not chosen to be very long, they represent a good approximation in the slanted case. Equations (5-7) imply that

$$P_1\, P_2 = -\, B_1\, M_2 \tag{5-8a}$$

or

$$(P_1\, P_2)\, H_1 = -\, M_2 \tag{5-8b}$$

These last two relations allow us to compute B or H following any of the already known procedures for filter estimation, since M_2 and the product $P_1 P_2$ can be regarded as an input-output pair. In the time domain, all the products in (5-8) are replaced by convolutions.

Next we will discuss some practical aspects of the computation of equations (5-8).

5.2. Gating the Primaries and the Multiples

In the problem of multiples suppression where usually a prediction is subtracted from the original seismogram, the correct timing of the variables involved is critical. In our case however, we require only a reasonable gating of the primaries (P_1 and P_2) and the multiple (M_2) in equations (5-8) . Since picking the primary gate is not a major problem, the situation reduces to correctly predicting the multiples arrivals.

In the case of a flat sea bottom, the problem is trivial and the first order multiple should arrive at twice the primary time, unless the location of $t = 0$ was not well-defined in the records. Even in this case, the inconvenience can be easily corrected.

If the sea bottom is irregular, the travel time associated with each bounce can vary from path to path, especially at large angles of propagation (stacking). The situation is illustrated in Figures 5.2 and 5.3. Figure 5.2 shows the same section of Chapter 4 (Figures 4.8,9) but for a plane wave that propagates from left to right at 15 degrees, as indicated in the upper-left corner. A program designed to pick up primary and multiple arrivals from this section was run under the assumption that the multiple arrived at twice the primary

travel time. The resulting gates are shown in Figure 5.3. Toward the flat portion of the data the program did a reasonable job, but in the left dipping part it missed the multiple practically everywhere.

In order to get the proper result, a correction has to be made to account for both the slanted propagation and the dipping of the sea bottom. The slanted migration theory previously developed correctly models these arrivals, and it is only a matter of running the forward problem, using the primary gate as input, to predict the arrival times of the multiples. Appendix 2 includes a simple ray approximation analysis of the situation and Figures 5.4 and 5.5 illustrate the results of such analysis. Taking into account the slanted propagation, but not the dip, we obtain the gates shown in Figure 5.4. The result is much better than the one in Figure 5.3 but still the multiple is missed in those places where the dip is significant. Finally, in Figure 5.5 we incorporate both corrections according to the final relations of Appendix 2.

5.3. The Estimation of the Filters

Once the input and output in the filter equation (5-8) have been properly defined, we must consider what algorithm we shall use in order to compute the filters B or H. We could follow the standard procedure of minimizing the L_2 norm. For equation (5-8) that means minimizing the quadratic form

$$E = \min_{B_1} |M_2 B_1 + P_1 P_2|^2 \qquad (5\text{-}9)$$

However, we have to include the following considerations:

1) The length of the gates is going to be rather short, thus we expect serious end-effects by just truncating P_1 , P_2 and M_2 (appending zeros at the end). A more general treatment of end-effects could be achieved by using a procedure of the type of Burg spectral estimation.

2) We must give a greater weight to the beginning of the gates, where the information is going to be less polluted. This applies especially to the multiple gates, where it is important not to have new primaries within the gate. A weighted least square procedure, with the beginning of the gates emphasized over its ends, accounts for this requirement.

3) The presence of noise in P and M could cause a large amount of noise in the predicted B . Thus we would like to add some constraints to the algorithm which tend to drive down the total power (including noise) in B while maintaining a low power in $P_1 P_2 + B_1 M_2$.

The last two conditions are met, if instead of (5-9), we minimize the more general quadratic form

$$E = \min_{B_i} \Sigma w_i \left| (M_2 B_i + P_1 P_2) \right|^2 + \Sigma w_i \left| (B_i - \bar{B}_i) \right|^2 \qquad (5\text{-}10)$$

where w_i are the weights and $\bar{B}_i$ the default solutions for B_i . In our case we can make $\bar{B}_i$ equal to an average of earlier estimations

of B_i . A Levinson shaping filter calculation, reorganized to resemble the Burg spectral estimation procedure according to the constraints in (5-10), was used in order to compute the following examples.

5.4. Synthetic and Field Data Examples

The model shown in Figure 5.6 was intended to test the proposed technique under conditions as close as possible to a real data situation. Figure 5.6a shows a portion of the slant stacked section computed in the previous chapter, corresponding to an angle of propagation of 20°. A synthetic model of reflection coefficients mimicking the field data was produced as shown in Figure 5.6b. It includes 4 dipping reflectors with laterally varying reflection coefficients and a relatively large noisy background. In the figure, for display purposes, the actual model was low-pass filtered.

A reflection seismogram was computed by running the forward 1-D problem with parameters equivalent to those of the actual field data (Figure 5.6a). Each of the obtained traces was further convolved with the direct arrivals of the corresponding field data traces. These direct arrivals were taken from the near offset traces of each gather and are shown in Figure 5.7a. The convolution was done in the frequency domain, thus adding some extra numerical noise. The final seismogram is shown in Figure 5.6c. It is evident that the dips and background noise are greatly exaggerated in relation to the original

Figure 5.6. A realistic synthetic model. Frame (a) shows a portion of the section in Figure 4.8. A synthetic model intended to reproduce few of the reflectors in (a) is shown in (b) . The actual model is white, but for display purposes it was low-pass filtered. Frame (c) shows the result of the forward slanted problem taking as input this model and parameters equivalents to those of the field data in frame (a) . Each trace has been convolved with the corresponding direct arrivals in section 5.6(a). Another synthetic seismogram of model (b), without noise, is shown at the right of 5.6 (c) to help in the identification of primary and multiple arrivals.

field data of Figure 5.6a. To help in the identification of the primaries and multiples arrivals, a synthetic seismogram of the model without noise and waveforms is shown to the right of the colored synthetic seismogram.

With this computed seismogram as input data, the slanted Noah algorithm was run with gates 150 points long (600 msec.) and a filter length of 100 points (400 msec.). These values, of course, are greatly exaggerated in relation to those that we would use in a real data case. This was done because, first, we knew the model a priori and, secondly, the waveforms (the direct arrivals) were quite long (500 msec.). The estimated waveforms are displayed in Figure 5.7b. By comparing them with the initial direct arrivals in 5.7a, we can see a reasonably good estimation is obtained for the initial part of the wavelet, but as expected, the estimation worsens toward the end. Besides the approximate nature of the theory, that prohibits long gates and estimates, this is probably due to the applied weights which tend to emphasize the beginning of the gates in relation to their ends.

In Figure 5.8 we repeat the same calculations, but this time using the real slant stacked section of Figure 5.6a which is also shown in Figure 5.8a. For this case the gates were reduced to 100 points (400 msec.) and the filters to 50 points (200 msec.). The estimated waveforms are shown in Figure 5.9. As an evaluation of the estimations, the original section was deconvolved with these waveforms and the result is shown in Figure 5.8b. For display purposes

Figure 5.8. A field data example of source waveform estimation. This figure repeats the estimation procedure of Figures 5.6 and 5.7, but this time the original stacked section (Frame a) is used as input data. The estimated waveforms are shown in Figure 5.9. In order to evaluate the estimation, the original section was deconvolved with these waveforms and the result is shown in Frame (b). A low-pass filtered version of the deconvolved section is shown in Frame (c). The spiking of the reflectors is evident, especially near the bottom of the section. The energy present before $t = 0$, is due to the frequency domain deconvolution technique that was applied.

again, the deconvolved section was further low-pass filtered and the final result is shown in Figure 5.8c. We can see that most of the reflections have been considerably spiked. This is especially noticeable in the reflections near the bottom of the section, which in the original seismograms appear to be quite ringing. The precursory energy before the first arrival is typical of deconvolutions that are performed in the frequency domain.

Despite these encouraging results, a word of caution has to be added. The presence of long direct arrivals in the recorded gathers tends to imply long waveforms in the stacked section. The proposed technique however, does not allow for long estimates. This poses a serious question for the future of the approach, since after removing the estimated waveforms, we still probably are left with a long component of the original waveform. The use of the direct arrivals as a means of compressing the waveform, previously to its estimation, currently is being explored.

5.5. An Optimization Technique for Multiple Suppression and Waveform estimation

We end the chapter by presenting the preliminary tests of a different approach to multiple suppression and waveform estimation, which by itself or in conjunction with the theory above discussed, opens new perspectives for the problem. One of the major advantages of this approach is that both the waveform and the reflection coefficient sequence are estimated simultaneously through an algorithm much simpler than the one previously discussed. At the present the

technique has been developed only for the case of vertical propagation, but hopefully it can be extended to slanted propagations.

In the following we will implicitly assume that all the variables have been Z-transformed. Moreover, we will be talking about three types of seismograms:

1) The deconvolved or whitened Noah seismogram U, which is a seismogram where all the multiple reflections and the shot waveform have been removed. It corresponds to what we called reflection coefficient sequence in Chapter 2.

2) The colored Noah seismogram U' with multiples removed but not the waveform. If as before we designate the waveform as B, then we will have that $U' = B\,U$.

3) The recorded seismogram R, which contains both multiples and waveform.

With these notations, Riley showed that the basic Noah algorithm for vertical propagation can be written in Z-transforms as

$$U' = B\,U = B\,R\,/\,(B+R) \tag{5-11}$$

Knowing R and B, this relation allows us to compute U or U'. A poor estimate of B will produce a U' not totally free from surface multiples. Since the remaining multiples add power to the seismogram, we can expect that the minimization of $||U'||^2$ with respect to B, would improve the estimates of U'

and B . A non-linear least square approach to the problem leads to the minimization of the length of

$$U' + dU' = U' + (\partial U' / \partial B) dB = U' - U^2 dB \approx 0 \qquad (5\text{-}12)$$

Equation (5-12) again can be interpreted as a filter estimation problem for dB with U being the input and U' the output. Then a recursion can be organized according to the following scheme:

dB_i <--- U_i , U'_i , using equation (5-12) .

B_{i+1} <--- $B_i + dB_i$

U_{i+1} , U'_{i+1} <--- B_{i+1} , R_i , using Noah relation (5-11)

where i refers to the recursion number and not the vectors' components.

As one would expect, the choice of a "good" starting value is critical. One possibility is to try $B = 0$ or $B = 1, 0, 0, \ldots$ and then define U and U' through (5-11). Also we could try to start with $U = U' = R$ and then use (5-11) to define B . Finally we could start with the results of the previously discussed technique. The solution of the filter equation (5-12) can be obtained with an algorithm similar to that of paragraph 5.3.

In order to test the resolution of the technique and its ability to handle relatively complex situations, synthetic seismograms were produced according to the models and waveform shown in Figure 5.10.

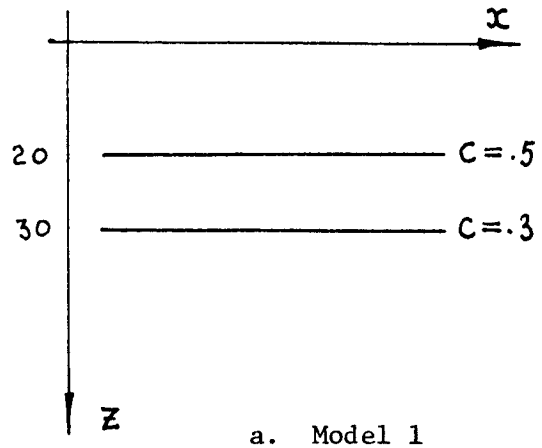

a. Model 1

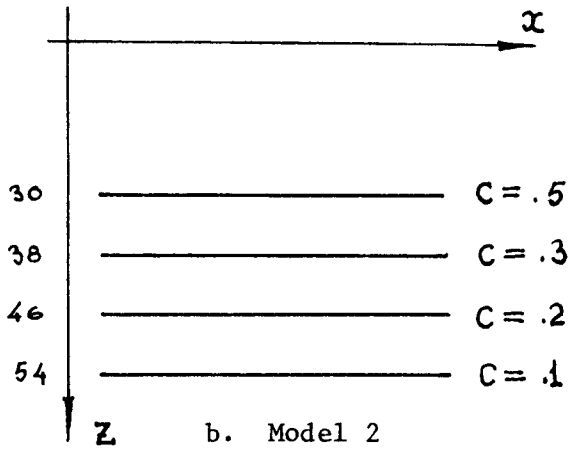

b. Model 2

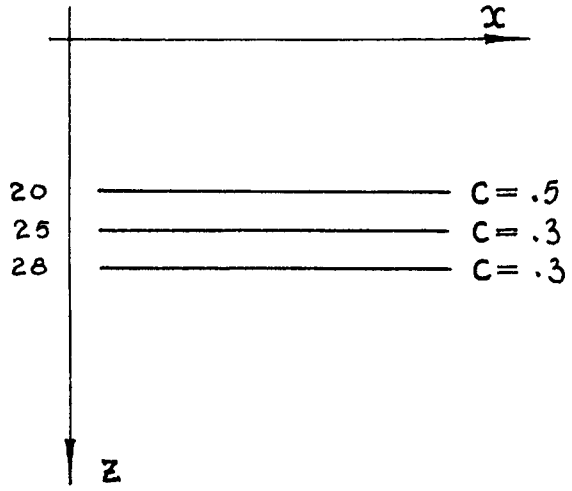

c. Model 3

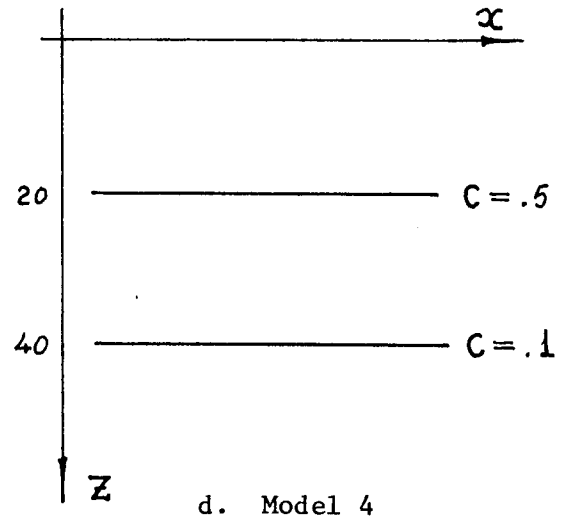

d. Model 4

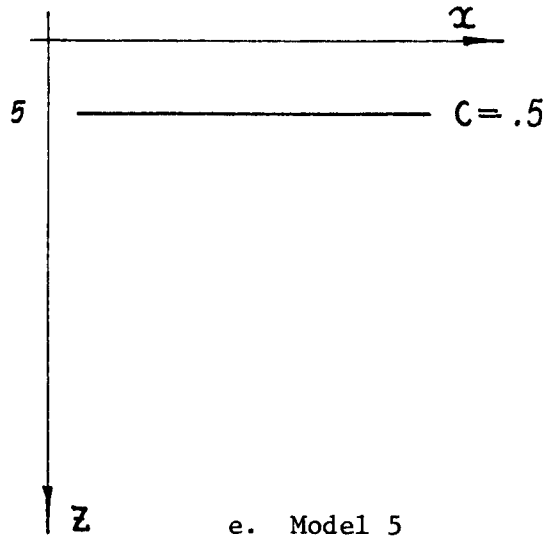

e. Model 5

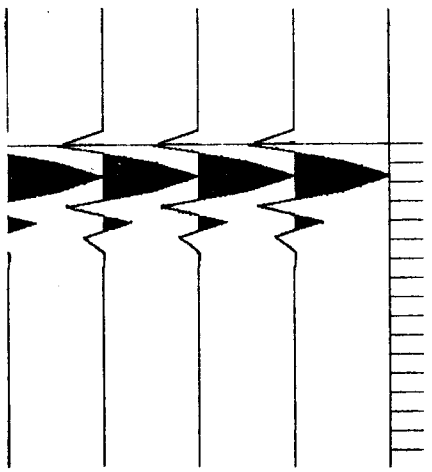

f. Synthetic shot waveform

B = (-.5,.5,1.,.5,-.4,.3,-.2)

Figure 5.10

A re-scaled, tapered version of the first primary was taken as an initial estimate for B. All the synthetic seismograms were made 150 points long and for display purposes were convolved with a three point binomial wavelet.

Model 1 is a "good" model, used mainly to test the technique in nearly optimal conditions. It took 9 iterations to achieve the desired degree of convergence ($||dB||/||B|| < 10^{-3}$). The results are shown in Figure 5.11.

Model 2 was used to test the degree of resolution in relation to the strength of the reflectors. As we see in Figure 5.12, the final U after 15 iterations is reasonably good and only the last reflector was lost. The estimated waveform is not as good as in the previous case, but this result could be greatly improved by extending the corresponding synthetic seismogram beyond 150 points.

Model 3 was meant to test resolution in terms of separation among reflectors. The first two reflectors are 5 points apart and the last one only 3 points apart (notice that the actual waveform is 7 points long). Figure 5.13 shows quite a good result both in terms of B and U.

Model 4 tries a complex situation, that is a small primary which coincides with the first multiple. As Figure 5.14 shows, our technique cannot handle this type of situation. The second reflector was lost in the final U and the estimated waveform is rather poor.

Finally Model 5 tried another type of difficulty, where we expected that this technique would be less sensitive than our previous one: shallow water. In this case the first multiple arrives before the first primary has died completely. Despite our expectations, the recursion flatly rejected the model: it diverged very quickly!

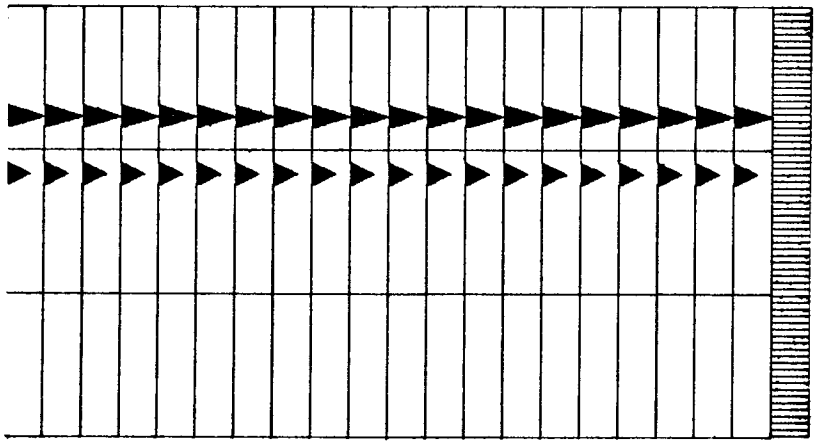

a. Model 1

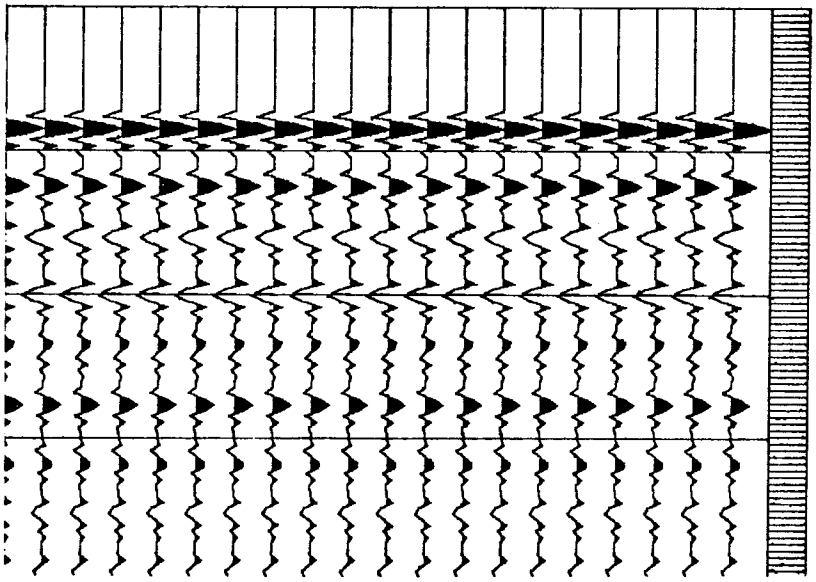

b. Synthetic seismogram

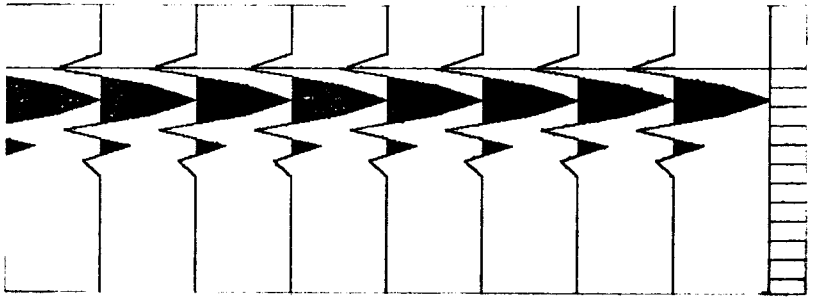

c. Synthetic shot waveform (-.5,.5,1.,.5,-.4,.3,-.2)

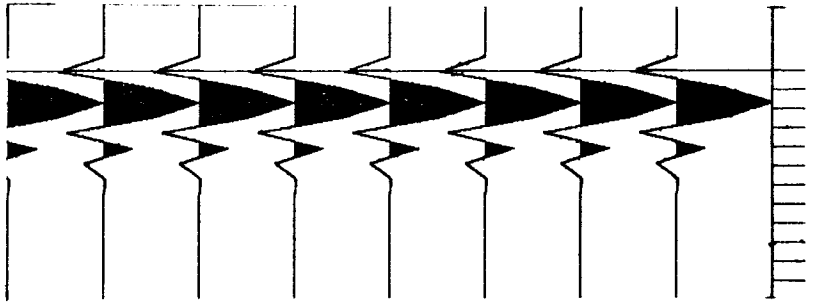

d. Estimated waveform

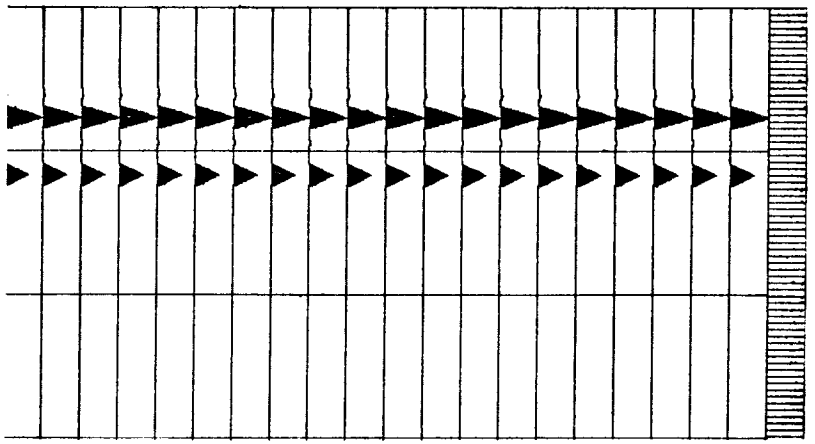

e. Estimated U (reflection coefficients).

Figure 5.11

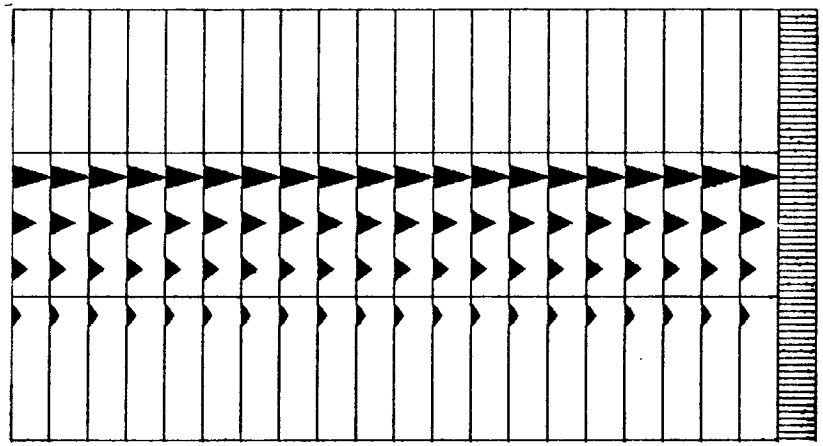

a. Model 2

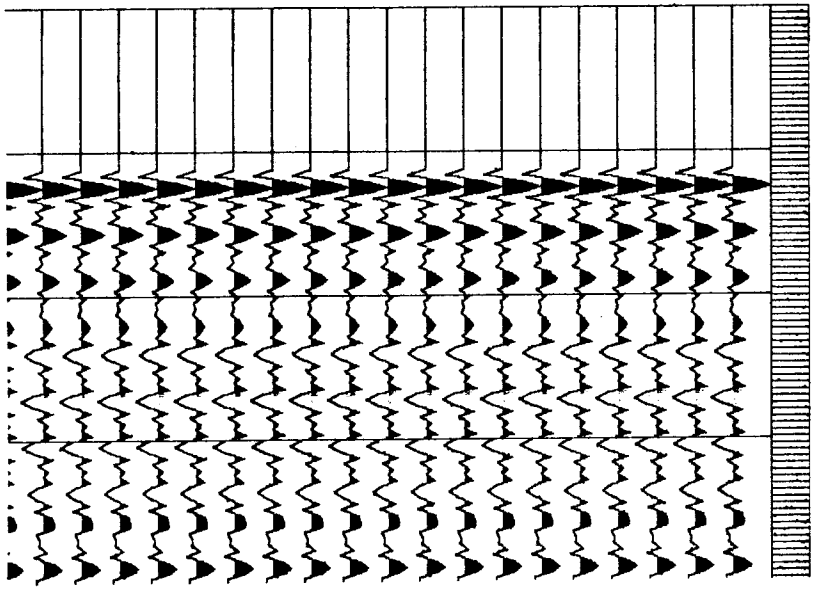

b. Synthetic seismogram

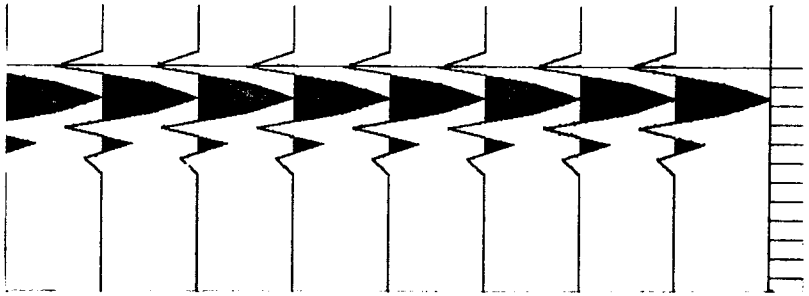

c. Synthetic shot waveform (-.5,.5,1.,.5,-.4,.3,-.2)

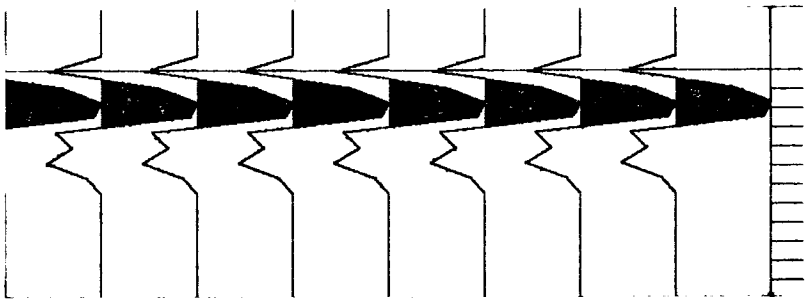

d. Estimated waveform

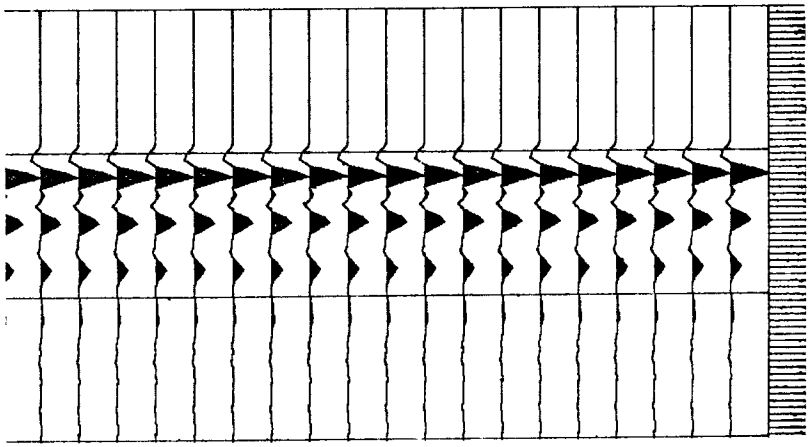

e. Estimated U (reflection coefficient)

Figure 5.12

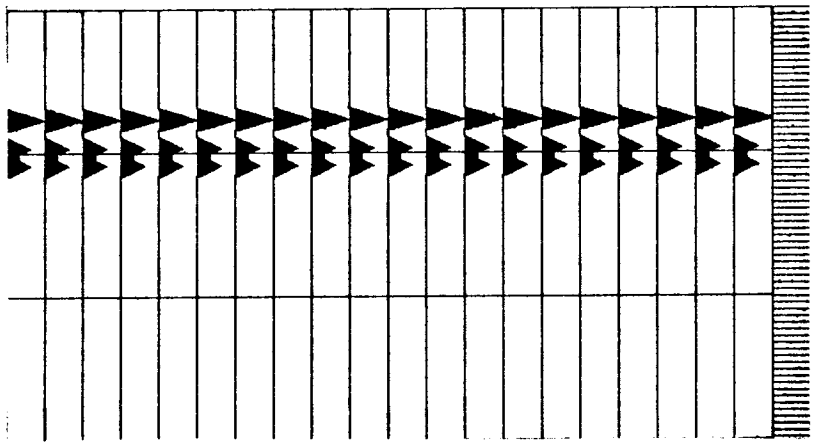

a. Model 3

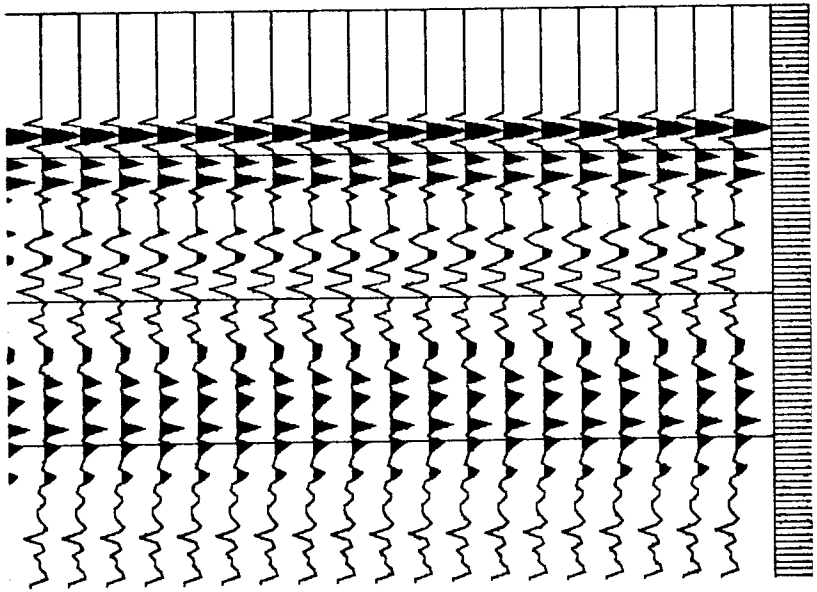

b. Synthetic seismogram

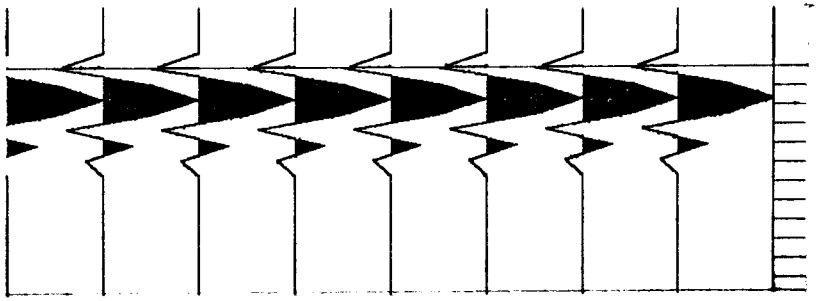

c. Synthetic shot waveform (-.5,.5,1.,.5,-.4,.3,-.2)

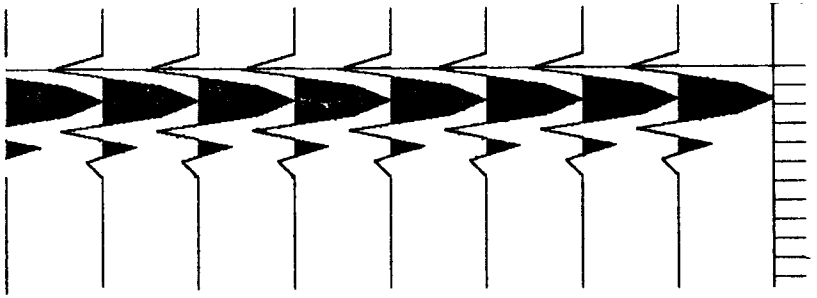

d. Estimated waveform

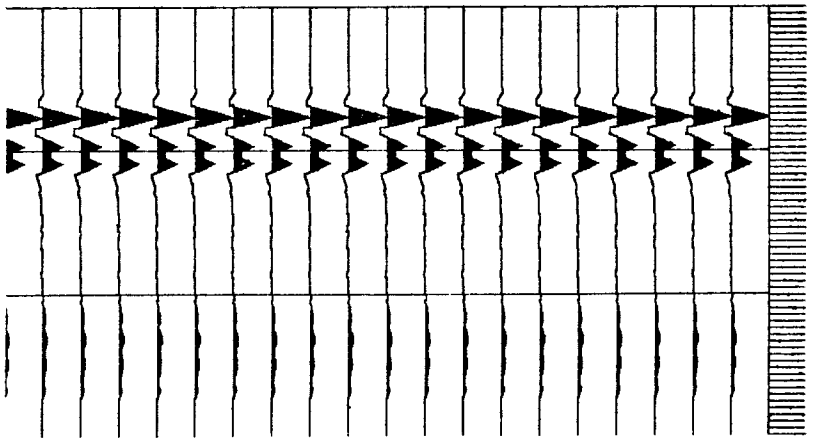

e. Estimated U (reflection coefficients)

Figure 5.13

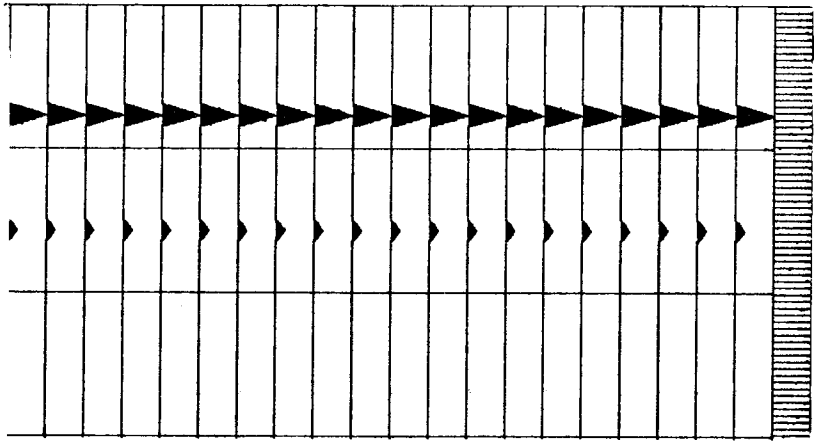

a. Model 4

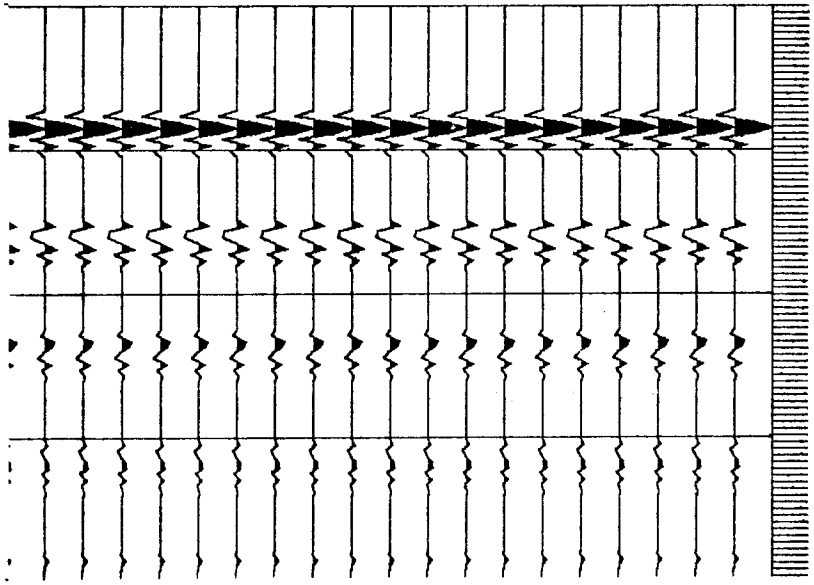

b. Synthetic seismogram

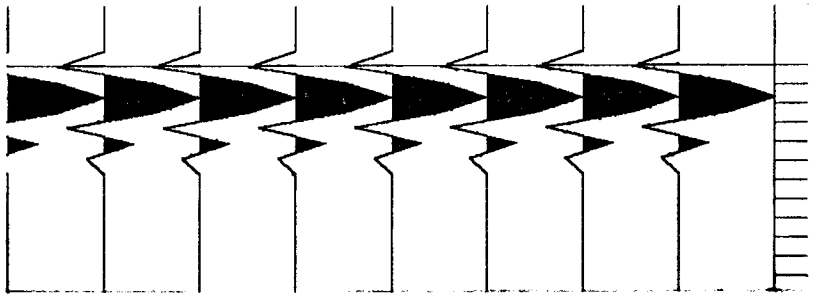

c. Synthetic shot waveform (-.5,.5,1.,.5,-.4,.3,-.2)

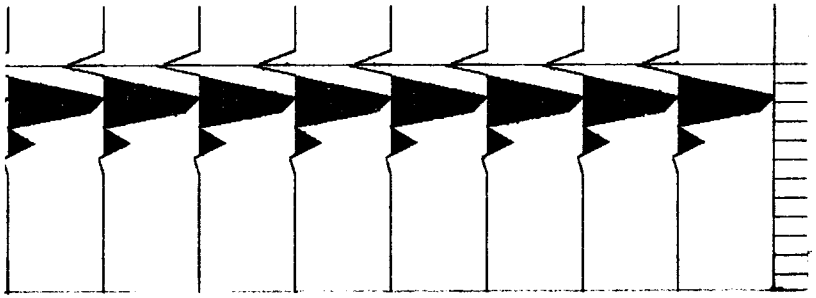

d. Estimated waveform

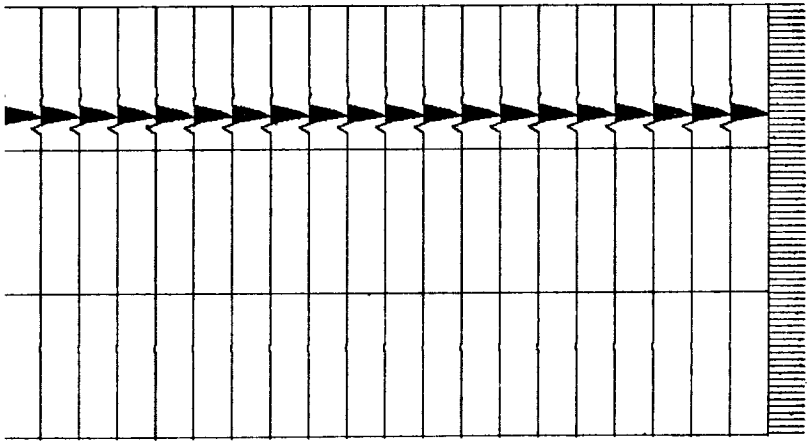

e. Estimated U (reflection coefficients)

Figure 5.14